Composites: Part A 149 (2021) 106559

Contents lists available at ScienceDirect

Composites Part A

journal homepage: www.elsevier.com/locate/compositesa

Significantly enhanced high permittivity and negative permittivity in Ag/Al_2O_3/3D-$BaTiO_3$/epoxy metacomposites with unique hierarchical heterogeneous microstructures

Mingli Han [a], Zhicheng Shi [a,*], Wenqiang Zhang [a], Kun Zhang [b], Huanlei Wang [a], Davoud Dastan [c], Runhua Fan [d]

[a] School of Materials Science and Engineering, Ocean University of China, Qingdao 266100, PR China
[b] Key Laboratory of Microgravity (National Microgravity Laboratory), Institute of Mechanics, Chinese Academy of Sciences, Beijing 100190, PR China
[c] Department of Materials Science and Engineering, Georgia Institute of Technology, Atlanta, Georgia 30332, USA
[d] Institute of Marine Materials Science and Engineering, Shanghai Maritime University, Shanghai 201306, PR China

ARTICLE INFO

Keywords:
Multifunctional composites
Polymer-matrix composites (PMCs)
Electrical properties
Interface

ABSTRACT

High dielectric permittivity materials are widely employed in various electronic devices. To satisfy the ongoing miniaturization of electronic devices, materials with further enhanced dielectric permittivities are strongly desired. In this work, a novel design of epoxy composites based on Ag/Al_2O_3/3D-$BaTiO_3$ foams with hierarchical heterogeneous microstructures are prepared. It is found that, the spatial distribution of the Ag particles can be easily controlled via adjusting the Ag^+/Al^{3+} mole ratios, yielding highly tailorable dielectric properties. When the Ag^+/Al^{3+} mole ratios are low, the Ag particles are well isolated by surrounding Al_2O_3, yielding the formation of numerous equivalent micro-capacitors and substantially enhanced dielectric permittivity. Moreover, the dielectric permittivities of the composites increase with higher Ag^+/Al^{3+} mole ratios. Consequently, a high dielectric permittivity of 160 @10 kHz, which is about 35 times that of the epoxy matrix, is achieved in the composite with a Ag^+/Al^{3+} mole ratio of 1.8. Meanwhile, a low tangent of about 0.062 is maintained. As the Ag^+/Al^{3+} mole ratio increases, the Ag particles become interconnected, forming Ag networks. Consequently, a plasma-like negative phenomenon which should be attributed to the plasma oscillation of free electrons in the percolative Ag networks, is observed. This work offers an effective route to design polymer composites with tailorable high permittivity and negative permittivity.

1. Introduction

In recent years, extensive attention has been devoted to the exploration of polymeric materials with high dielectric permittivity (high-*k*) because of their wide applications in antennas [1,2], electrostatic capacitors [3-6], sensors [7,8], and field-effect transistors [9,10], etc. Generally, the dielectric permittivity (ε_r) of polymers are very low (<10 @1 kHz) which are far below our expectations. Even for the ferroelectric polymer, such as polyvinylidene fluoride (PVDF) and its copolymers, it is also very difficult to achieve permittivities above 15 @1 kHz. With the aim of improving the ε_r of polymeric materials, numerous strategies have been proposed, among which introducing ferroelectric ceramic and electric conductive fillers into the polymers is a widely adopted one. However, these two types of fillers have their inherent disadvantages. For the composites with ferroelectric ceramic fillers, the enhancement of ε_r is very limited (<30 @ 1 kHz) even when the filler faction is up to 50 vol%, resulting in undesired high weight and poor mechanical property [11-14]. For the composites with electric conductive fillers, although ultrahigh ε_r (>1000 @ 1 kHz) can be achieved via controlling the filler fraction near the percolation threshold, the serious leakage conduction inevitably brings about sharply elevated loss (tanδ) [15-17].

Considering the inherent drawbacks of the ferroelectric ceramic and electric conductive fillers, much attention has been devoted to the optimization of fillers. For example, constructing core–shell structured fillers has been widely demonstrated to be an effective way to realize balanced permittivity and loss. Specifically, it is found that coating electric conductive fillers with insulating nanoparticles can avoid the direct contact of the conductive fillers, which effectively hinders the

* Corresponding author.
E-mail address: zcshi@ouc.edu.cn (Z. Shi).

https://doi.org/10.1016/j.compositesa.2021.106559
Received 20 May 2021; Received in revised form 21 June 2021; Accepted 11 July 2021
Available online 15 July 2021

formation of percolation networks and suppresses conduction loss [18-20]. Similarly, anchoring electric conductive nanoparticles on the surface of ferroelectric ceramic fillers has been proved to be capable of achieving enhanced permittivity without apparently elevating loss [21-23]. In addition to designing core–shell structured fillers, there are also other methods which can get concurrent high permittivity and low loss, including using disorderly mixed hybrid fillers composed of insulating and conductive components [24-26], constructing polymer composites co-filled with ferroelectric and conductive nanofillers [27-29]. Up to now, although huge efforts have been devoted to the optimization of fillers, the results are still not satisfactory. For instance, for most of the so far reported polymer composites, it remains difficult to simultaneously realize $\varepsilon_r > 100$ and $\tan\delta < 0.1$. In other words, much more attention should be paid to the further exploration of new and effective strategies for the design of high-*k* polymer composites.

It is worth noting that, Luo and coworkers [30] constructed a class of epoxy composites incorporated with three dimensional $BaTiO_3$ foams (3D-BT) rather than conventional $BaTiO_3$ nanoparticles (BTNPs). It is demonstrated that, the composite with 30 vol% 3D-BT exhibits a high ε_r of about 200 @1 kHz which is about 20 times that of its counterpart filled with randomly dispersed BTNPs. It is believed that the 3D-BT effectively facilitates the transportation of dipolar polarization, yielding substantially enhanced ε_r. Guo and coworkers [31] reported a unique design of epoxy composites based on oriented 3D-BT. A high ε_r of about 400 @10 kHz, which is approximately 10 times that of its counterpart filled with BTNPs, is obtained in the composite with 24 vol% 3D-BT. In addition to experimental researches, Feng and coworkers [32] also theoretically demonstrate that constructing polymer composites based on 3D ferroelectric ceramic networks is an effective way to achieve high permittivity. In our recent work, a design of hollow-structured 3D-BT foams are prepared and hosted in epoxy matrix, forming 3D-BT/epoxy composites. A high ε_r of about 126 along with a low loss of about 0.045 at 10 kHz are concurrently achieved in the composite with only 18 vol% 3D-BT [33].

As discussed above, constructing polymer composites incorporated with 3D ferroelectric ceramic networks is an effective way to achieve concurrent high permittivity and low loss. Targeting for further improving the dielectric performance of the epoxy composites based on hollow-structured 3D-BT, herein, silver (Ag) and alumina (Al_2O_3) particles are in-situ grown on the outer and inner surfaces of the hollow 3D-BT, forming Ag/Al_2O_3/3D-BT/epoxy composites with hierarchical heterogenetic interfaces. It is interesting to found that, in comparison with 3D-BT/epoxy composites, the introduction of Ag and Al_2O_3 results in substantially enhanced ε_r without sacrificing the low loss. Meanwhile, the Ag/Al_2O_3/3D-BT/epoxy composites based on 3D-BT exhibit much higher ε_r and lower loss than their counterparts based on randomly dispersed $Ag/Al_2O_3/BaTiO_3$ hybrid particles. Besides, a distinct percolation process along with an interesting negative ε_r phenomenon is observed, and the underlying mechanism is further explored.

2. Experimental

2.1. Materials

Nickel foam (350 g/m^2, Hefei Kejing Material Technology Co., Ltd.), barium titanate ($BaTiO_3$, 300 nm, > 99.5 %, Shandong Sinocera Functional Material Co., Ltd.), poly(ethylenimine) (PEI, M.W.10000, 99 %, Aladdin Industrial Corporation), isopropyl alcohol (≥99.7 %, Sinopharm Chemical Reagent Co., Ltd.), acetone (≥99.7 %, Sinopharm Chemical Reagent Co., Ltd.), anhydrous ethanol (≥99.7 %, Sinopharm Chemical Reagent Co., Ltd.), epoxy resin Epon828 (Hexion Specialty Chemicals. Curing agent), methyltetrahydrophthalic anhydride (99.0 %, anhydride group content ≥ 41.0 %, Shanghai Macklin Biochemical Technology Co., Ltd.), 2-ethyl-4-methylimidazole (99 %, Shanghai Macklin Biochemical Technology Co., Ltd.), iron trichloride hexahydrate ($FeCl_3{\cdot}6H_2O$, AR, ≥ 99.0 %, Sinopharm Chemical Reagent Co., Ltd.), silver nitrate ($AgNO_3$, ≥ 99.8 %, AR, Sinopharm Chemical Reagent Co., Ltd.) and Aluminum nitrate nonahydrate ($Al(NO_3)_3{\cdot}9H_2O$, AR, ≥ 99.0 %, Sinopharm Chemical Reagent Co., Ltd.) were purchased, which were used in experiments without any further purification.

2.2. Fabrication of 3D-$BaTiO_3$ foam

As illustrated in Fig. 1 3D-$BaTiO_3$ (3D-BT) were prepared by an electrophoretic deposition process (EPD) combined with high temperature sintering. Firstly, the impurities of nickel foam were removed by acetone, deionized water and anhydrous ethanol under sonication. Secondly, $BaTiO_3$ suspensions were prepared by adding $BaTiO_3$ powders into 50 mL isopropyl alcohol and sonicated for 20 min. Thirdly, the $BaTiO_3$ nanoparticles were in-situ formed on the wall of the porous nickel foam by EPD, in which the nickel foam is used as the cathode and the deposition voltage is 40 V. Subsequently, the nickel foam coated by $BaTiO_3$ was sintered at 1200 ℃ for 2 h in a tubular furnace under argon atmosphere. Then the sintered samples were soaked in 1 mol/L of $FeCl_3$ solution to remove the nickel foams. Finally, the obtained 3D-BT foams were calcined at 700 °C for 2 h in the muffle furnace. Then the weight of the 3D-BT foams (m_1) were measured.

2.3. Fabrication of Ag/3D-$BaTiO_3$ and Ag/Al_2O_3/3D-$BaTiO_3$ foams

The Ag/3D-$BaTiO_3$ (Ag/3D-BT) foams were fabricated by an impregnation method (Fig. 1), and the specific steps are as follows. To begin, solutions with different molar concentrations of $AgNO_3$ were prepared. Then the 3D-BT foams were immersed in the $AgNO_3$ solution and vacuumed for 20 min followed by drying at 100 °C for 2 h in the oven. After that, the samples were calcined in the muffle furnace at 700 °C for 2 h in air, forming the Ag/3D-BT foams. Finally, the weight of the Ag/3D-BT foams (m_2) were measured and the weight of Ag can be expressed as (m_2-m_1). In this work, the Ag content is controlled via adjusting the concentration of Ag^+ in the impregnation solution. The fabrication process of Ag/Al_2O_3/3D-BT foams is the same as that of Ag/3D-BT foams and the only difference is that the mixed solutions of $AgNO_3$ and $Al(NO_3)_3$ with different mole ratios (i.e., 1:1, 1.2:1, 1.4:1, 1.6:1 and 1.8:1) rather than pure $AgNO_3$ solution, are used in the impregnation process. Then, the 3D-BT foams were immersed in the solution of $AgNO_3$ and $Al(NO_3)_3$ under vacuum for 20 min followed by drying at 100 °C for 2 h in the oven. Finally, the dried samples were calcined at 700 °C for 2 h in the muffle furnace, forming the Ag/Al_2O_3/3D-BT foams.

2.4. Fabrication of Ag/Al_2O_3/3D-BT/epoxy composites

The Ag/Al_2O_3/3D-BT/epoxy composites were prepared via a vacuum infiltration process. Typically, the epoxy resin, methyltetrahydrophthalic anhydride and 2-ethyl-4-methylimidazole were mixed at a mass ratio of 10:8:0.1 and stirred at 50 °C and 70 °C for 30 min, respectively. Next, the epoxy solution was vacuumed at room temperature for 20 min to remove bubbles. Then, the porous Ag/3D-BT and Ag/Al_2O_3/3D-BT foams were infiltrated with epoxy and cured at 100 °C for 6 h in vacuum oven, forming the Ag/3D-BT/epoxy and Ag/Al_2O_3/3D-BT/epoxy composites. Finally, the weight of the Ag/3D-BT/epoxy composites (m_3) were measured. The filling fractions of BT and Ag in Ag/3D-BT/epoxy composites can be expressed as m_1/m_3 and (m_2-m_1)/m_3, respectively.

2.5. Characterization

The morphologies and elemental distributions of the composites were observed by scanning electron microscopy (SEM, S-4800, Hitachi, Ltd.) equipped with energy-dispersive spectrometer (EDS). The compositions of the composites were analyzed by using an X-ray diffractometer (XRD, D8 Advance, Bruker, Ltd.). The ε_r and $\tan\delta$ were

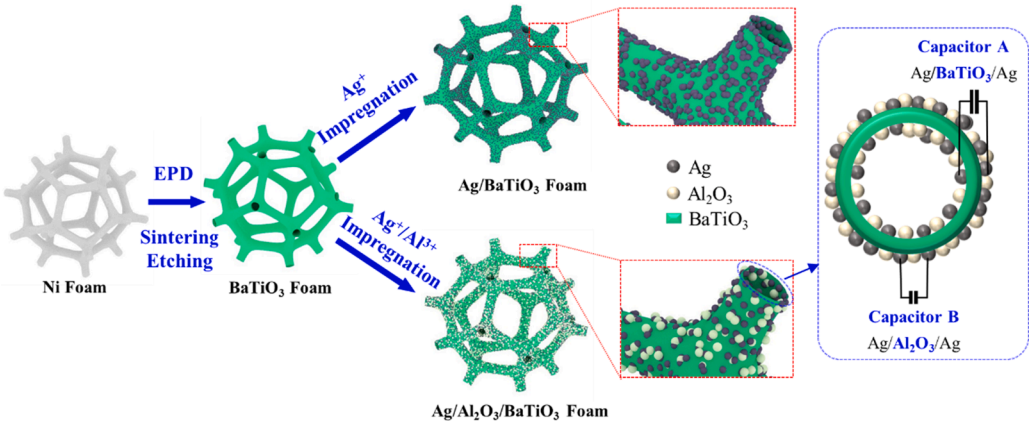

Fig. 1. Schematic fabrication process of the Ag/3D-$BaTiO_3$ and Ag/Al_2O_3/3D-$BaTiO_3$ foams, as well as the formation of equivalent micro-capacitors.

measured by an Agilent E4980A Precision LCR analyzer under an AC voltage of 100 mV at room temperature in the frequency range from 5 kHz to 1 MHz. Before dielectric measurements, circular gold electrodes with a diameter of 2.98 mm were sputtered on the two sides of the composite films. The ε_r were calculated by the formula specified as: $\varepsilon_r = tC_p/A\varepsilon_0$, where t is the thickness of the sample, A is the area of the electrode, ε_0 is the absolute dielectric constant of free space (8.85×10^{-12}F/m), C_p is the measured capacitance. The breakdown strength measurements were carried out by using a setup equipped with a Treck 610C amplifier under a voltage ramping rate of 500 V/s at room temperature (PolyK Technologies, USA). The discharge energy densities (U_d) were calculated from the *P-E* loops, which were obtained by a ferroelectric test system based on a modified Sawyer-Tower circuit (PolyK Technologies, USA).

3. Results and discussion

The X-ray diffraction (XRD) patterns of the foams at different preparation steps are presented in Fig. 2. As shown in Fig. 2**a**, pure $BaTiO_3$ (JCPDS PDF No.01–074-4540) foam is obtained without the appearance of nickel and other additional phase, indicating that nickel foam has been totally removed during the etching process and no unexpected reaction takes place during the calcination treatment. Furthermore, the diffraction peaks at 41.1°, 47.5°, 64.2° and 75.9° can be ascribed to the characteristic reflections of Ag at (111), (200), (220) and (311). (Fig. 2**b**). It should be noted that, the intensity of the diffraction patterns of $BaTiO_3$ in the Ag/$BaTiO_3$ foam is much weaker than that of the pure $BaTiO_3$ foam in Fig. 2**a** because of the fact that the $BaTiO_3$ foam is covered by Ag. Fig. 2**c** shows the XRD patterns of the foam after the impregnation of $AgNO_3$/$Al(NO_3)_3$ mixed solution with subsequent calcination. Distinct diffraction peaks of Ag and Al_2O_3 are observed without the appearance of other undesired phases, indicating that $AgNO_3$ and $Al(NO_3)_3$ are totally converted into Ag and Al_2O_3.

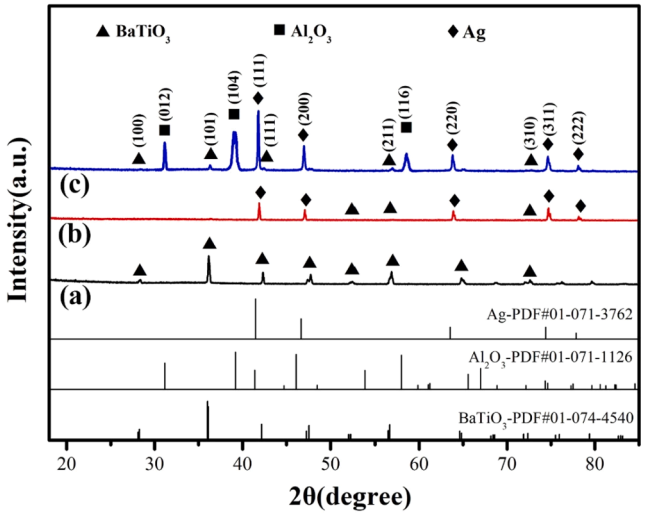

Fig. 2. XRD patterns of hollow structured 3D-$BaTiO_3$ foam (a), Ag/3D-$BaTiO_3$ composite foam with 1 vol% Ag (b), and Ag/Al_2O_3/3D-$BaTiO_3$ composite foam with 1 vol% Ag (c).

The morphologies of the 3D foams, epoxy composites, as well the elemental mapping analysis results are presented in Fig. 3. We can see that, a porous 3D-BT foam composed of hollow $BaTiO_3$ tubes is successfully fabricated (Fig. 3**a and d**). After the $AgNO_3$ solution impregnation process, Ag particles are homogeneously loaded onto the 3D-BT foam (Fig. 3**b**). After the $AgNO_3$/$Al(NO_3)_3$ mixed solution impregnation process, Ag and Al_2O_3 are co-deposited onto the outer and inner surfaces of 3D-BT foam (Fig. 3**c, e, g,** **Figure S1**). We can also see that the average diameter of the Ag particles in Fig. 3**c and g** is larger than that in Fig. 3**b** because of the higher Ag^+ concentration in the impregnation solution. As displayed in Fig. 3**f**, after the vacuum infiltration process, both of the outer and inner pores of the foam are totally infiltrated with epoxy without the appearance of observable voids and other defects, which is beneficial to high dielectric permittivity and high breakdown strength.

The ac conductivities (σ_{ac}) of the epoxy composites at varied frequencies are further studied. As shown in Fig. 4**a and b**, the σ_{ac} of the Ag/3D-BT/epoxy composites increase with higher Ag content. Especially, a sharp enhancement of σ_{ac} from 2×10^{-3} S/m to 2.29×10^{2} S/m is observed when the Ag content increases from 0.8 vol% to 1 vol%. This phenomenon should be attributed to the formation of percolative Ag networks [34,35]. Moreover, the Ag content also has significant influences on the frequency dependences of the composites. Specifically, the σ_{ac} of the composites with Ag contents below 1 vol% increase with increasing frequency f and the σ_{ac}-f relationships follow the power law $\sigma_{ac} = Kf^n (0 < n < 1)$, where K is the scale coefficient, n is the exponent, indicating a hopping conduction mechanism [36]. On the contrary, the σ_{ac} of the composite with 1 vol% Ag decreases as a function of frequency, which is attributed to the skin effects of the current in the percolative Ag networks [37]. As shown in **Figure S4**, the σ_{ac} of the Ag/Al_2O_3/3D-BT/epoxy composites with 1 vol% Ag and varied contents of Al_2O_3 show much lower σ_{ac} than the Ag/3D-BT/epoxy composites with 1 vol% Ag, revealing that the introduction of Al_2O_3 effectively hinders the formation of Ag networks. Furthermore, the decrease of σ_{ac} as a result of higher Al_2O_3 also indicates that the Ag particles are well separated by Al_2O_3, which will also be demonstrated by the SEM analysis in the following discussions.

Fig. 5**a and b** show the frequency dependences of dielectric

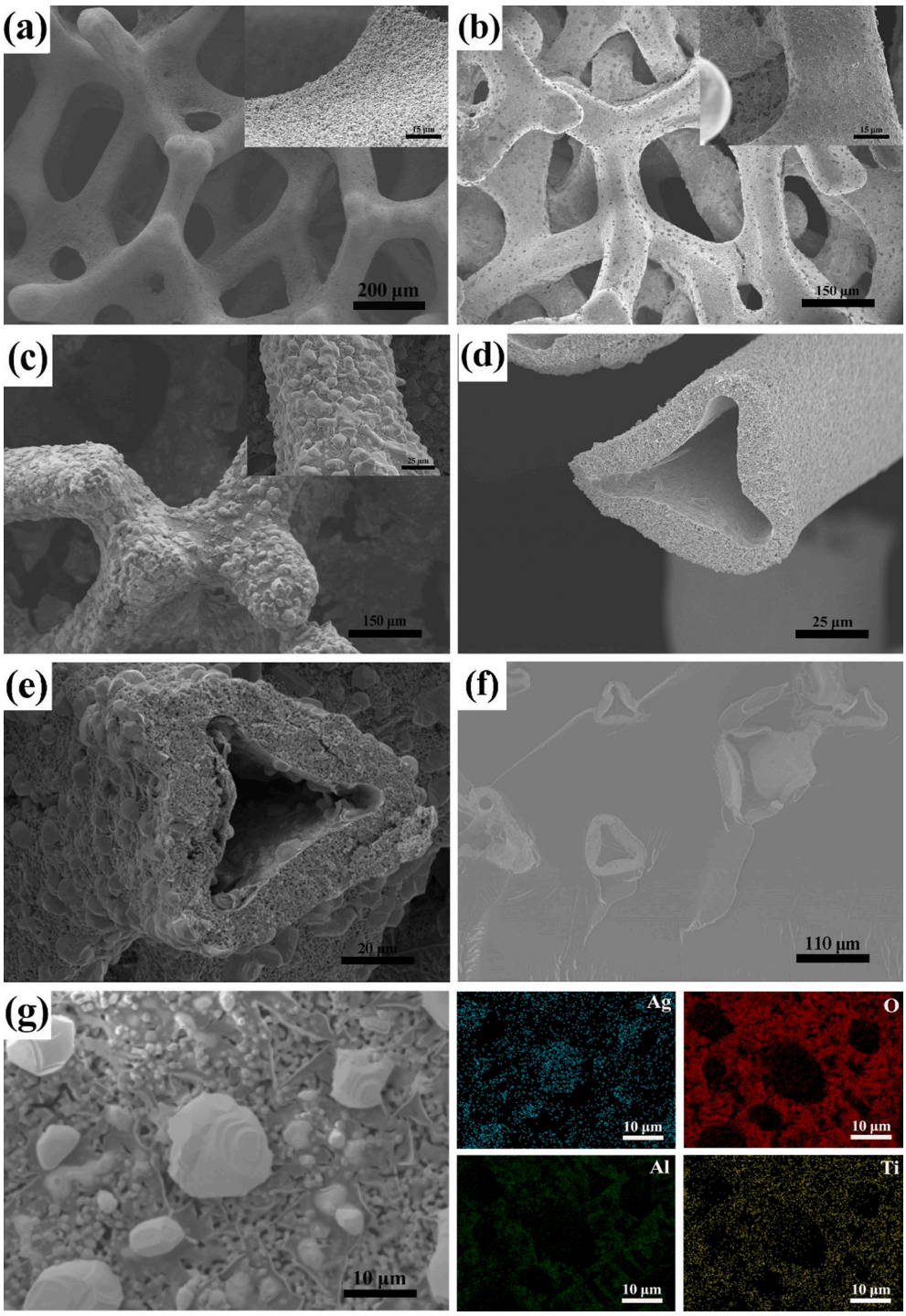

Fig. 3. Surface SEM images of 3D-$BaTiO_3$ foam (a), Ag/3D-$BaTiO_3$ foam with 0.2 vol% Ag (b), and Ag/Al_2O_3/3D-$BaTiO_3$ foam with 1 vol% Ag (c). Fractured cross-sectional SEM images of 3D-$BaTiO_3$ foam (d), Ag/Al_2O_3/3D-$BaTiO_3$ foam with 1 vol% Ag (e) and Ag/Al_2O_3/3D-$BaTiO_3$/epoxy composite with 1 vol% Ag. The high magnification surface SEM image of Ag/Al_2O_3/3D-$BaTiO_3$ foam with 1 vol% Ag (g) and corresponding elemental mapping analysis.

permittivity ε_r and loss tangent tanδ for pure epoxy (EP) and the Ag/3D-BT/epoxy composites with different contents of Ag particles. Clearly, the 3D-BT/epoxy composite with 5 vol% $BaTiO_3$ exhibits a greatly improved ε_r in comparison with pure EP, which has been widely reported in various $BaTiO_3$/polymer composites and should be attributed to the strong dipolar polarization of $BaTiO_3$ [38,39]. It is worth noting that, the introduction of Ag particles results in obviously enhanced ε_r along with well maintained low loss (tanδ < 0.03 @10 kHz, Fig. 5**b**) and the ε_r increases with increasing Ag content. Specifically, the ε_r of the composite with 0.8 vol% Ag becomes up to 71 @10 kHz which is about 245 % that of the 3D-BT/epoxy composite without Ag particles. The huge heterogenetic interfaces between Ag particles, 3D-BT foam, and epoxy matrix can efficiently store charges when the composite is under an external electric field, resulting in improved ε_r. Interestingly, a unique plasma-like negative ε_r appears when the Ag content reaches 1 vol%. Meanwhile, an obvious percolation behavior is observed, indicating the formation of 3D Ag networks. Drude model is usually used to describe the plasma-like negative permittivity behavior [40,41]:

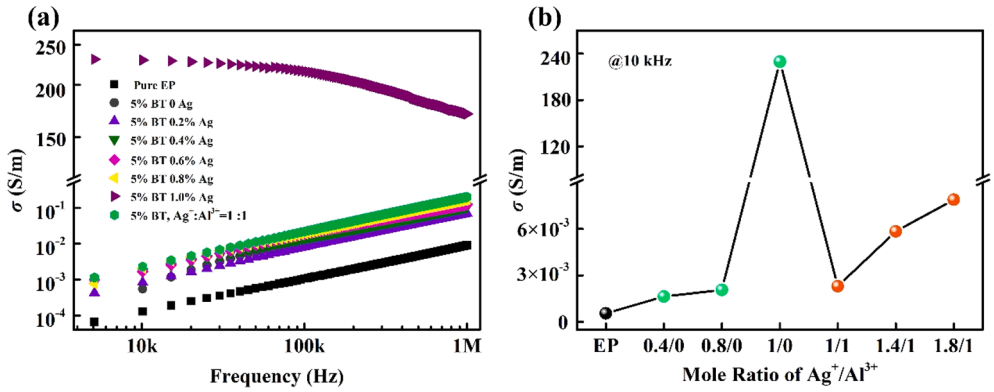

Fig. 4. (a) Frequency dependences of ac conductivities of the Ag/3D-$BaTiO_3$/epoxy and Ag/Al_2O_3/3D-$BaTiO_3$/epoxy composites. (b) The variation of ac conductivity with Ag^+/Al^{3+} mole ratios.

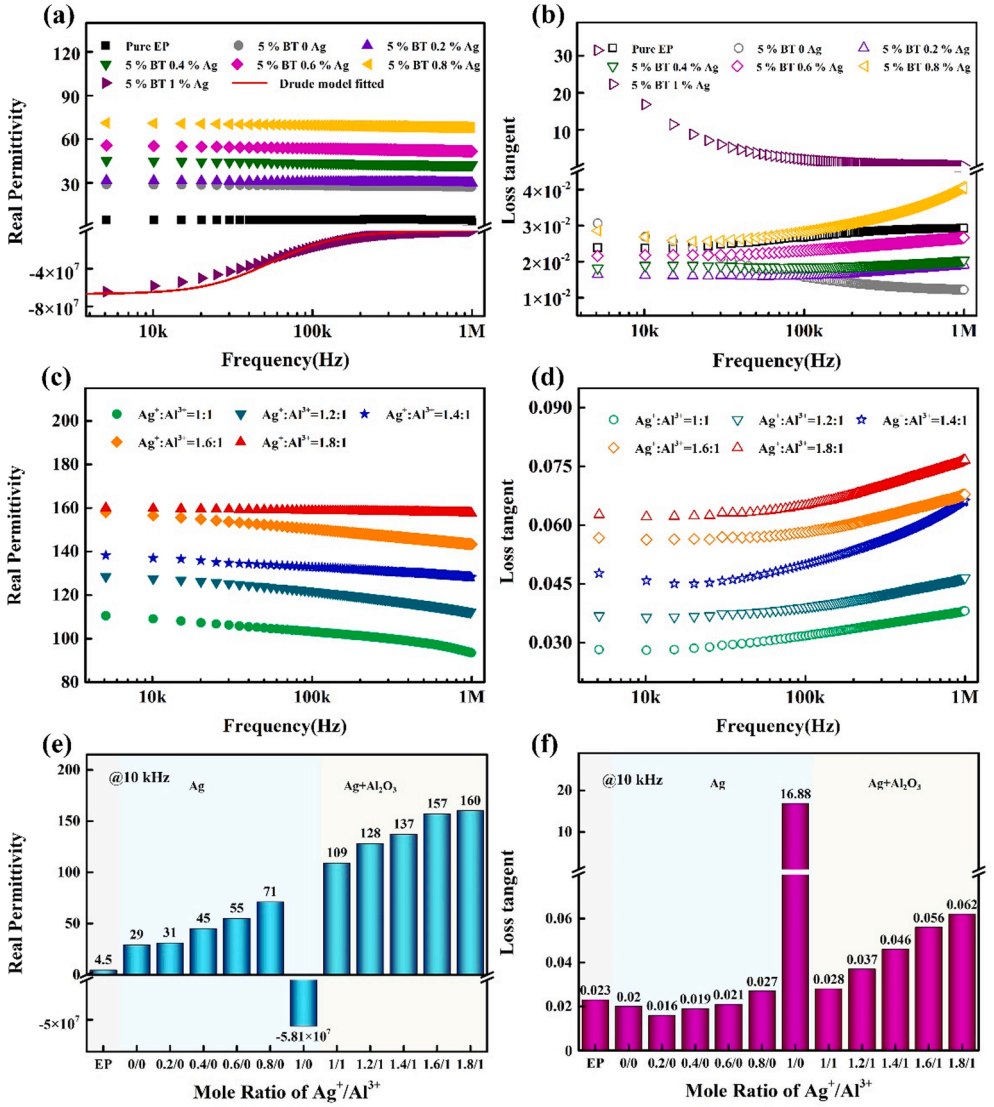

Fig. 5. The frequency dependences of dielectric permittivity and the fitted curve using Drude model (a) and low tangent (b) of pure epoxy and the epoxy composites containing 3D-$BaTiO_3$ and Ag/3D-$BaTiO_3$. The frequency dependences of dielectric permittivity (c) and low tangent (d) of the epoxy composites containing Ag/Al_2O_3/3D-$BaTiO_3$ with different Ag^+/Al^{3+} mole ratios. The variation of dielectric permittivity (e) and loss tangent (f) with Ag^+/Al^{3+} mole ratios.

$$\varepsilon^{'}{}_{\mathrm{r}}(\omega) = 1 - \frac{{\omega_{\mathrm{p}}}^2}{\omega^2 + {\omega_{\tau}}^2} \quad (1)$$

$$\omega_{\mathrm{p}} = \sqrt{\frac{n_{\mathrm{eff}} e^2}{m_{\mathrm{eff}} \varepsilon_0}} \quad (2)$$

where ω_p ($\omega_p = 2\pi f_p$) is the angular plasma frequency, ω ($\omega = 2\pi f$) is the angular frequency of applied electric field, ω_τ is the damping parameter, ε_0 is permittivity of vacuum, n_{eff} is the effective concentration of conduction electrons, m_{eff} is the effective weight of an electron, and e is the charge of electron (1.6×10^{-19}C). As can be seen, the dielectric spectra of the composite agrees well with the Drude model (solid line in Fig. 5**a**)

fitted curve using fits well with the original data, revealing that the negative ε_r is originated from the plasma oscillation of delocalized electrons throughout the Ag networks [40,41]. The negative permittivity composite has huge potential for electromagnetic shielding applications [42,43].

Fig. 5**c and d** display the dielectric performances of the Ag/Al_2O_3/3D-BT/epoxy composites with varied Ag^+/Al^{3+} mole ratios. It can be seen that, negative ε_r can no longer be observed in the Ag/Al_2O_3/3D-BT/epoxy composites with 1 vol% Ag. Instead, significantly enhanced positive ε_r along with substantially suppressed tanδ is observed, indicating that percolative Ag networks are destroyed because of the addition of Al_2O_3 which has been demonstrated by the SEM images (Fig. 3**c, g**). Specifically, a high ε_r of 160 @10 kHz, which is about 516 %, 356 %, 291 %, 225 % that of the Ag/3D-BT/epoxy composites with 0.2 vol%, 0.4 vol %, 0.6 vol%, 0.8 vol% Ag, is achieved (Fig. 5**e**). Meanwhile, a low tanδ of 0.062 is maintained (Fig. 5**f**) because the Ag particles are isolated by Al_2O_3. As illustrated in Fig. 1, there exist hierarchical heterogenetic interfaces between the Ag, Al_2O_3, $BaTiO_3$ and epoxy in the Ag/Al_2O_3/3D-BT/epoxy composites. As a result, two types of equivalent micro-capacitors (i.e., (A) Ag/$BaTiO_3$/Ag capacitor in which Ag acts as the electrodes and $BaTiO_3$ acts as the dielectric; (B) Ag/Al_2O_3/Ag capacitor in which Ag acts as the electrodes and Al_2O_3 acts as the dielectric.) are formed. The numerous equivalent micro-capacitors effectively enhance the charge storage capability of the composites, yielding the obviously improved ε_r. Meanwhile, the Ag particles are separated by Al_2O_3, which effectively avoids the formation of percolative Ag networks, resulting in the low loss. The dielectric properties of our composites are further compared with other reported results as displayed in Table 1 [11,44-49]. We can see that, for most of the so far reported results, it is still difficult to concurrently achieve $\varepsilon_r > 100$ and tan$\delta < 0.1$. In this work, the composites with hierarchical equivalent micro-capacitors exhibit outstanding comprehensive dielectric performances (e.g., high ε_r of 109 and 160 corresponding to low tanδ of 0.028 and 0.062, respectively), which demonstrates that this design strategy is capable of achieving well balanced high ε_r and low tanδ.

In practical applications, much attention should also be paid to the insulating performances of dielectric materials, especially for high voltage applications. Therefore, the breakdown performances of the composites are further studied using a two-parameter Weibull distribution model [11]:

$$P(\mathrm{E}) = 1 - \exp[-(\frac{\mathrm{E}}{\alpha})^{\beta}] \quad (3)$$

where $P(E)$ is the probability of breakdown, E is the experimentally obtained breakdown electric field, α is the Weibull breakdown strength

Table 1
Comparison of the dielectric performances of reported results and this work.

High-k composites	ε_r	tanδ	References
20 vol% $BaTiO_3$/HT	12	0.02	[11]
6 wt% MXene@AgNPs/P(VDF-HFP)	650	1.5	[44]
30 vol% BT NPs/PVDF	27	0.015	[45]
1.082 wt% sLTNO@mAC/Epoxy	150	0.35	[46]
10 wt% Fe_3O_4 @$BaTiO_3$/ P(VDF-HFP)	15.5	0.05	[47]
TiO_2-BT-TiO_2@dopa/PVDF	12	0.04	[48]
0.61 vol% rGO/12.5 vol% CCTO/PVDF	40	0.085	[49]
Ag/Al_2O_3/$BaTiO_3$/Epoxy1 vol %Ag, Ag^+/Al^{3+}=1:1	109	0.028	This work
Ag/Al_2O_3/$BaTiO_3$/Epoxy1 vol% Ag, Ag^+/Al^{3+}=1.8:1	160	0.062	This work

E_b (the electric field at which there is a 63.2 % probability of failure), and β is a shape parameter reflecting the reliability of the tested data (the slope of the derived logarithm function) and higher β implies better reliability. Fig. 6**a and b** show the Weibull distribution of breakdown electric field and the variation of E_b with the Ag^+/Al^{3+}mole ratio. We can see that, the E_b decreases with higher Ag^+/Al^{3+} mole ratio because higher Ag content will result in decreased distance between Ag particles, which could facilitate the formation and development of breakdown paths. In particular, when the Ag content exceeds some critical values (e.g., percolation threshold), the Ag particles cannot be well isolated by Al_2O_3, leading to the partial agglomeration of the Ag particles and obviously reduced E_b. Dielectric materials are widely employed in electrostatic capacitors, so the dielectric capacitive energy storage performances of the composites are further studied. Fig. 6**c and d** display the discharged energy density U_d and charge/discharge efficiency η, which are derived from the ferroelectric hysteresis loops (*P-E* loops). It can be seen from Fig. 6**c** that the composites possess obviously enhanced U_d compared with pure epoxy under the same charging electric field. Specifically, the composite with a Ag^+/Al^{3+} mole ratio of 1.8 exhibits a U_d of about 4.8×10^{-2} J/cm^3 which is about 240 % that of pure epoxy ($\sim 2 \times 10^{-2}$ J/cm^3). However, the composites with high Ag contents cannot be charged to high voltages because of their low E_b. Consequently, the composite with a Ag^+/Al^{3+} mole ratio of 1.4 possesses the highest U_d of about 7.85×10^{-2} J/cm^3 under an electric field of 30 kV/mm, which is about 180 % that of pure epoxy ($\sim 4.35 \times 10^{-2}$ J/cm^3). As shown in Fig. 6**d**, pure epoxy possesses the highest η (>85 %), while the composite with a Ag^+/Al^{3+} mole ratio of 1.8 has the lowest η (<75 %). The reduced η with increasing Ag^+/Al^{3+} mole ratio should be ascribed to the elevated conduction loss originated from the partially interconnected Ag particles. As discussed above, the composites exhibit superior capacitive energy storage performances, and could be promising candidates for pulsed power capacitors.

For comparison, a series of epoxy composites filled with randomly dispersed Ag/Al_2O_3/BT hybrid particles are further prepared. As displayed in Fig. 7 **and S2**, the composites with randomly dispersed Ag/Al_2O_3/BT hybrid fillers show much lower ε_r in comparison with their counterparts based on 3D fillers. This phenomenon should be attributed to the fact that, much higher loading fractions of filler are required in the composites with randomly dispersed hybrid fillers, in comparison with the composites with 3D fillers, to form 3D filler networks to ensure the continuous transmission of polarization. Moreover, as for the Ag/Al_2O_3/BT foam, the Ag and Al_2O_3 are in-situ formed on the BT foam, which ensures their uniform distributions. On the contrary, there may exist severe agglomerations between Ag/Al_2O_3/BT hybrid particles, resulting in unstable and deteriorated dielectric performances. The breakdown behaviors of these two types of composites based on Ag/Al_2O_3/3D-BT foams and Ag/Al_2O_3/BT hybrid particles are further compared. As shown in Fig. 7 **and S3**, when the Ag^+/Al^{3+} mole ratio is low (i.e., 1, 1.2 and 1.4), the composites based on Ag/Al_2O_3/3D-BT foams exhibit much higher E_b than their counterparts with Ag/Al_2O_3/BT hybrid particles. When the Ag^+/Al^{3+} mole ratio is high (i.e., 1.6 and 1.8), these two types of composites have comparable E_b. This phenomenon should be attributed to the different spatial distributions of Ag particles in these two types of composites. Specifically, when the Ag content is low (i.e., low Ag^+/Al^{3+} mole ratio), the Ag particles on the 3D-BT foams are well separated by Al_2O_3, while the Ag particles may interconnect with each other in the composites with Ag/Al_2O_3/BT hybrid particles. When the Ag content is high, the Ag particles on the 3D-BT foams become partially interconnected which is similar to the situation in the composites filled with Ag/Al_2O_3/BT hybrid particles. This work provides a new design strategy to construct polymer composites with hierarchical heterogenetic interfaces to achieve concurrent high dielectric permittivity and low loss.

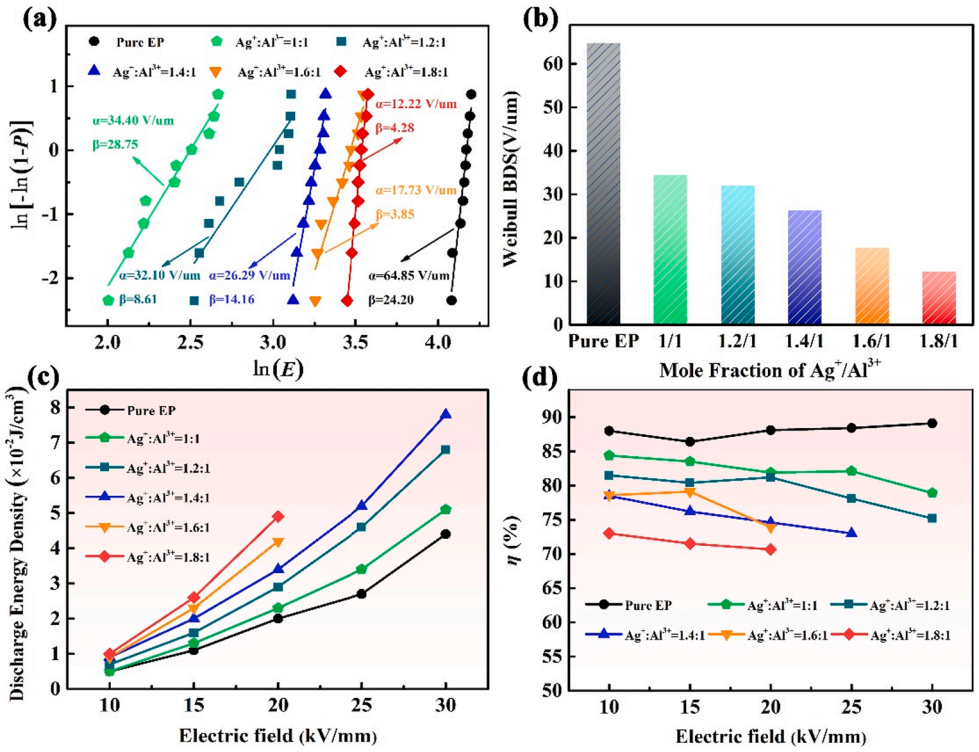

Fig. 6. Weibull distribution of the tested breakdown electric fields (a), characteristic breakdown strengths (b), discharge energy densities (c) and discharge efficiencies (d) of the Ag/Al_2O_3/3D-BT/epoxy composites incorporated with 3D-BT foams.

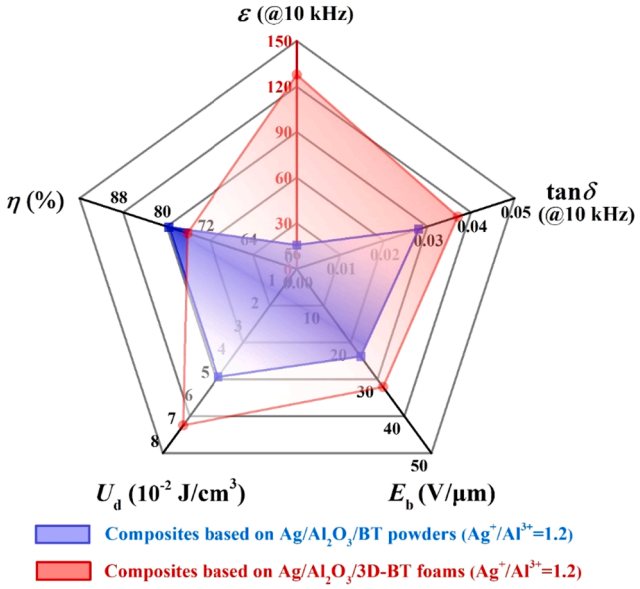

Fig. 7. The comparison of the dielectric performances of the composites based on Ag/Al_2O_3/3D-BT foam and Ag/Al_2O_3/BT hybrid powders.

4. Conclusion

In summary, Ag/Al_2O_3/3D-$BaTiO_3$/epoxy composites with unique hierarchical heterogeneous microstructures are fabricated via a facile wet impregnation technique along with a calcination process. It is found that, numerous hierarchical equivalent micro-capacitors, in which Ag acts as the electrodes while the Al_2O_3, $BaTiO_3$ and epoxy act as the insulating dielectrics, are formed in the composites. Therefore, substantially enhanced dielectric permittivities are achieved. Meanwhile, the Ag particles are isolated by surrounding Al_2O_3, resulting well maintained low loss. In addition, the dielectric performances are highly tunable with the Ag^+/Al^{3+} mole ratios. Consequently, a high dielectric permittivity of 160 @10 kHz, which is about 35 times that of the epoxy matrix, is achieved in the composite with a Ag^+/Al^{3+} mole ratio of 1.8. Moreover, as the Ag^+/Al^{3+} mole ratio increases, an interesting negative permittivity phenomenon appears and is believed to be originated from the plasma oscillation of free electrons in the percolative Ag networks. This work offers an effective strategy to achieve enhanced high permittivity without sacrificing low loss and is also of great significance for the design of negative permittivity metacomposites.

CRediT authorship contribution statement

Mingli Han: Conceptualization, Data curation, Investigation, Methodology, Validation, Writing - original draft. **Zhicheng Shi:** Conceptualization, Validation, Resources, Supervision, Writing - review & editing. **Wenqiang Zhang:** Writing - review & editing. **Kun Zhang:** Writing - review & editing. **Huanlei Wang:** Resources, Supervision, Writing - review & editing. **Davoud Dastan:** Writing - review & editing. **Runhua Fan:** Resources, Supervision.

Declaration of Competing Interest

The authors declare that they have no known competing financial interests or personal relationships that could have appeared to influence the work reported in this paper.

Acknowledgements

The authors acknowledge the financial support of this work by National Natural Science Foundation of China (51773187), The Fundamental Research Funds for the Central Universities (201961060).

Appendix A. Supplementary material

Supplementary data to this article can be found online at https://doi.org/10.1016/j.compositesa.2021.106559.

References

[1] Gan G, Zhang D, Li J, Wang G, Huang X, Yang Y, et al. Matching impedance of Cd-substituted magnesium ferrites for wideband and miniaturized antennas. Ceram Int 2020;46(18):27996–8005.

[2] Yang Y, Zhang H, Li J, Rao Y, Wang G, Gan G. Bi^{3+} doping-adjusted microstructure, magnetic, and dielectric properties of nickel zinc ferrite ceramics for high frequency LTCC antennas. Ceram Int 2020;46(16):25697–704.

[3] Zhou L, Zhou Y, Shi Y, Chen T, Zou T, Zhou D, et al. Enhancing thermal stability of P(VDF-HFP) based nanocomposites with core-shell fillers for energy storage applications. Compos Sci Technol 2020;186:107934. https://doi.org/10.1016/j.compscitech.2019.107934.

[4] Rout SK, Anwar S, Tripathy BC. Nanosilver Coated coir based dielectric materials with high *k* and low Df for embedded capacitors and insulating material applications–a greener approach. ACS Sustain Chem Eng 2019;7(4):3824–37.

[5] Luo H, Zhang D, Jiang C, Yuan Xi, Chen C, Zhou K. Improved dielectric properties and energy storage density of poly(vinylidene fluoride-co-hexafluoropropylene) nanocomposite with hydantoin epoxy resin coated $BaTiO_3$. ACS Appl Mater Interfaces 2015;7(15):8061–9.

[6] Zhang D, Liu W, Guo Ru, Zhou K, Luo H. High discharge energy density at low electric field using an aligned titanium dioxide/lead zirconate titanate nanowire array. Adv Sci 2018;5(2):1700512. https://doi.org/10.1002/advs.201700512.

[7] Shen Xi, Zheng Q, Kim J-K. Rational design of two-dimensional nanofillers for polymer nanocomposites toward multifunctional applications. Prog Mater Sci 2021;115:100708. https://doi.org/10.1016/j.pmatsci.2020.100708.

[8] Ko Y, Yoon H, Kwon S, Lee H, Park M, Jeon I, et al. Elastomeric high-*k* composites of low dielectric loss tangent: experiment and simulation. Compos Part B Eng 2020;201:108337.

[9] Wang B, Huang W, Chi L, Al-Hashimi M, Marks TJ, Facchetti A. High-*k* gate dielectrics for emerging flexible and stretchable electronics. Chem Rev 2018;118(11):5690–754.

[10] Lill AT, Eftaiha AF, Huang J, Yang H, Seifrid M, Wang M, et al. High-*k* fluoropolymer gate dielectric in electrically stable organic field-effect transistors. ACS Appl Mater Interfaces 2019;11(17):15821–8.

[11] Jiang Z-H, Li W-D, Yang X, Chen Xi, Wang C, Chen M-Y, et al. Low dielectric loss and high breakdown strength photosensitive high-*k* composites containing perfluoroalkylsilane treated $BaTiO_3$ nanoparticles. Compos Part B Eng 2020;192:108013. https://doi.org/10.1016/j.compositesb:2020.108013.

[12] Lu Xu, Zou X, Shen J, Jin Li, Yan F, Zhao G, et al. Characterizations of P(VDF-HFP)-$BaTiO_3$ nanocomposite films fabricated by a spin-coating process. Ceram Int 2019;45(14):17758–66.

[13] Chen CT, Wang L, Liu XM, Yang WL, Lin JQ, Chen GR, et al. K0.5Na0.5NbO3-SrTiO3/PVDF polymer composite film with low remnant polarization and high discharge energy storage density. Polymers 2019;11:310.

[14] Luo H, Roscow J, Zhou X, Chen S, Han X, Zhou K, et al. Ultra-high discharged energy density capacitor using high aspect ratio $Na_{0.5}Bi_{0.5}TiO_3$ nanofibers. J Mater Chem A 2017;5(15):7091–102.

[15] Li Y, Zhang D, Wang S, Zhan Y, Yin J, Tao X, et al. Fe_3O_4 decorated graphene/poly (vinylidene fluoride) nanocomposites with high dielectric constant and low dielectric loss. Compos Sci Technol 2019;171:152–61.

[16] Li W, Song Z, Qian J, Tan Z, Chu H, Wu X, et al. Enhancing conjugation degree and interfacial interactions to enhance dielectric properties of noncovalent functionalized graphene/poly (vinylidene fluoride) composites. Carbon 2019;141:728–38.

[17] Hu J, Zhang S, Tang B. 2D filler-reinforced polymer nanocomposite dielectrics for high-*k* dielectric and energy storage applications. Energy Storage Mater 2021;34:260–81.

[18] Zhang Q-P, Zhu W-F, Liang D-M, Wu X-L, Chen R-C, Sun N, et al. Core-shell structured $CaCO_3$@CNF for enhanced dielectric properties of polymer nanocomposites. Appl Surf Sci 2019;487:77–81.

[19] Zhu X, Yang J, Dastan D, Garmestani H, Fan R, Shi Z. Fabrication of core-shell structured Ni@$BaTiO_3$ scaffolds for polymer composites with ultrahigh dielectric constant and low loss. Compos Part A Appl Sci Manuf 2019;125:105521. https://doi.org/10.1016/j.compositesa:2019.105521.

[20] Jiang Y, Zhang Z, Zhou Z, Yang H, Zhang Q. Enhanced dielectric performance of P(VDF-HFP) composites with satellite–core-structured Fe_2O_3@$BaTiO_3$ nanofillers. Polymers 2019;11(10):1541. https://doi.org/10.3390/polym11101541.

[21] Chen G, Lin X, Li J, Huang S, Cheng X. Core-satellite ultra-small hybrid Ni@BT nanoparticles: a new route to enhanced energy storage capability of PVDF based nanocomposites. Appl Surf Sci 2020;513:145877. https://doi.org/10.1016/j.apsusc.2020.145877.

[22] Prateek, Singh D, Singh N, Garg A, Gupta RK. Engineered thiol anchored Au-$BaTiO_3$/PVDF polymer nanocomposite as efficient dielectric for electronic applications. Compos Sci Technol 2019;174:158–68.

[23] Wang H, Xie H, Wang S, Gao Z, Li C, Hu G-H, et al. Enhanced dielectric property and energy storage density of PVDF-HFP based dielectric composites by incorporation of silver nanoparticles-decorated exfoliated montmorillonite nanoplatelets. Compos Part A Appl Sci Manuf 2018;108:62–8.

[24] Sahoo G, Sarkar N, Swain SK. The effect of reduced graphene oxide intercalated hybrid organoclay on the dielectric properties of polyvinylidene fluoride nanocomposite films. Appl Clay Sci 2018;162:69–82.

[25] Pawar SP, Melo G, Sundararaj U. Dual functionality of hierarchical hybrid networks of multiwall carbon nanotubes anchored magnetite particles in soft polymer nanocomposites: simultaneous enhancement in charge storage and microwave absorption. Compos Sci Technol 2019;183:107802. https://doi.org/10.1016/j.compscitech.2019.107802.

[26] Yin P, Shi ZC, Sun L, Xie PT, Sun K, Fan RH, et al. Improved breakdown strengths and energy storage properties of polyimide composites: the effect of internal interfaces of C/SiO_2 hybrid nanoparticles. Polymer Compos 2021:1–11.

[27] Li W, Song Z, Qian J, Tan Z, Chu H, Wu X, et al. Largely enhanced dielectric and thermal conductive properties of novel ternary composites with small amount of nanofillers. Compos Sci Technol 2018;163:71–80.

[28] Cui Y, Zhang T, Feng Yu, Zhang C, Chi Q, Zhang Y, et al. Excellent energy storage density and efficiency in blend polymer-based composites by design of core-shell structured inorganic fibers and sandwich structured films. Compos Part B Eng 2019;177:107429. https://doi.org/10.1016/j.compositesb:2019.107429.

[29] Guo F, Shen Xi, Zhou J, Liu D, Zheng Q, Yang J, et al. Highly thermally conductive dielectric nanocomposites with synergistic alignments of graphene and boron nitride nanosheets. Adv Funct Mater 2020;30(19):1910826. https://doi.org/10.1002/adfm.v30.1910.1002/adfm.201910826.

[30] Luo S, Shen Y, Yu S, Wan Y, Liao W-H, Sun R, et al. Construction of a 3D-$BaTiO_3$ network leading to significantly enhanced dielectric permittivity and energy storage density of polymer composites. Energy Environ Sci 2017;10(1):137–44.

[31] Guo Ru, Roscow JI, Bowen CR, Luo H, Huang Y, Ma Y, et al. Significantly enhanced permittivity and energy density in dielectric composites with aligned $BaTiO_3$ lamellar structures. J Mater Chem A 2020;8(6):3135–44.

[32] Feng Y, Liang P, Tang B, Wang Y, Liu J, Shui L, et al. Construction of particle network for ultrahigh permittivity of dielectric polymer composite toward energy devices: a molecular dynamics study. Nano Energy 2019;64:103985. https://doi.org/10.1016/j.nanoen.2019.103985.

[33] Yang J, Zhu X, Wang H, Wang X, Hao C, Fan R, et al. Achieving excellent dielectric performance in polymer composites with ultralow filler loadings via constructing hollow-structured filler frameworks. Compos Part A Appl Sci Manuf 2020;131:105814. https://doi.org/10.1016/j.compositesa:2020.105814.

[34] Song S, Wang Y, Luo Yu, He D, Abella A, Deng Y. One-dimensional oriented microcapacitors in ternary polymer nanocomposites: toward high breakdown strength and suppressed loss. Mater Des 2018;140:114–22.

[35] Hou Z-L, Liu X-D, Song W-L, Fang H-M, Bi S. Graphene oxide foams: the simplest carbon-air prototypes for unique variable dielectrics. J Mater Chem C 2017;5(13):3397–407.

[36] Schrøder TB, Dyre JC. AC hopping conduction at extreme disorder takes place on the percolating cluster. Phys Rev Lett 2008;101(2). https://doi.org/10.1103/PhysRevLett.101.025901.

[37] Liu G, Chen Yi, Gong M, Liu X, Cui Z-K, Pei Q, et al. Enhanced dielectric performance of PDMS-based three-phase percolative nanocomposite films incorporating a high dielectric constant ceramic and conductive multi-walled carbon nanotubes. J Mater Chem C 2018;6(40):10829–37.

[38] Li Z, Shen Z, Yang X, Zhu X, Zhou Y, Dong L, et al. Ultrahigh charge-discharge efficiency and enhanced energy density of the sandwiched polymer nanocomposites with poly(methyl methacrylate) layer. Compos Sci Technol 2021;202:108591. https://doi.org/10.1016/j.compscitech.2020.108591.

[39] Cao M, Li L, Hong WB, Wu SY, Chen XM. Greatly enhanced permittivity in $BaTiO_3$-epoxy dielectric composites with improved connectivity of ceramic phase. J Materiomics 2021;7(1):1–7.

[40] Shi Z-C, Fan R-H, Zhang Z-D, Qian L, Gao M, Zhang Mo, et al. Random composites of nickel networks supported by porous alumina toward double negative materials. Adv Mater 2012;24(17):2349–52.

[41] Shi Z-C, Fan R-H, Yan K-L, Sun K, Zhang M, Wang C-G, et al. Preparation of iron networks hosted in porous alumina with tunable negative permittivity and permeability. Adv Funct Mater 2013;23(33):4123–32.

[42] Cheng C, Jiang Y, Sun X, Shen J, Wang T, Fan G, et al. Tunable negative permittivity behavior and electromagnetic shielding performance of silver/silicon nitride metacomposites. Compos Part A Appl Sci Manuf 2020;130:105753. https://doi.org/10.1016/j.compositesa:2019.105753.

[43] Wang Z, Sun K, Xie P, Hou Q, Liu Y, Gu Q, et al. Design and analysis of negative permittivity behaviors in barium titanate/nickel metacomposites. Acta Mater 2020;185:412–9.

[44] Ma W, Yang Ke, Wang H, Li H. Poly(vinylidene fluoride-co-hexafluoropropylene)-MXene nanosheet composites for microcapacitors. ACS Appl Nano Mater 2020;3(8):7992–8003.

[45] Jian G, Jiao Y, Meng QZ, et al. Hydrothermal synthesis of $BaTiO_3$ nanowires for high energy density composite capacitors. J Mater Sci 2020;55:6903–14.

[46] Peng BH, Yuan L, Liang GZ, Gu AJ. Getting self-healing ability and ultra-low dielectric loss for high-k epoxy resin composites through building networks based on Li0.3Ti0.02Ni0.68O grafted carbon nanotube bundles with unique surface architecture. Appl Surface Sci 2021;536:147955.

[47] Zhou L, Zhou YF, Shi YC, Chen TW, Zou TH, Zhou DX, et al. Enhancing thermal stability of P(VDF-HFP) based composites with core-shell fillers for energy storage applications. Compos Sci Technol 2020;186:107934.
[48] Prateek BR, Siddiqui S, Garg A, Gupta RK. Significantly enhanced energy density by tailoring the interface in hierarchically structured TiO_2-$BaTiO_3$-TiO_2 nanofillers in PVDF-based thin-film polymer composites. ACS Appl Mater Interfaces 2019;11(15):14329–39.
[49] Chen Z, Liu Y, Fang L, Jiang P, Huang X. Role of reduced graphene oxide in dielectric enhancement of ferroelectric polymers composites. Appl Surface Sci 2019;470:348–59.